Original Article

FOXP3 promotes colorectal carcinoma liver metastases by evaluating MMP9 expression via regulating S-adenosylmethionine metabolism

Zhe Wang, Jingdong Zhang

Medical Oncology Department of Gastrointestinal Cancer, Liaoning Cancer Hospital & Institute, Cancer Hospital of China Medical University, Shenyang 110042, China

Contributions: (I) Conception and design: J Zhang; (II) Administrative support: Z Wang; (III) Provision of study materials or patients: Z Wang; (IV) Collection and assembly of data: Z Wang; (V) Data analysis and interpretation: Z Wang; (VI) Manuscript writing: All authors; (VII) Final approval of manuscript: All authors.

Correspondence to: Jingdong Zhang, PhD. Medical Oncology Department of Gastrointestinal Cancer, Liaoning Cancer Hospital & Institute, Cancer Hospital of China Medical University, No. 44 Xiaoheyan Road, Dadong District, Shenyang 110042, China. Email: jdzhang@cancerhosp-ln-cmu.com.

Background: Growing evidence has proved that Forkhead box protein 3 (FOXP3), which is a master regulatory gene in the development and function of regulatory T-cells, is expressed in human cancer cells. This expression indicates the crucial role FOXP3 takes up as the disease progresses. However, its role in colorectal cancer (CRC) liver metastasis is still mostly unknown. This study set out to explore the molecular characteristics of FOXP3 in driving the liver metastasis within CRC.

Methods: We downloaded the RNA-seq data from the GSE50760. Weighted gene co-expression network analysis (WGCNA)WGCNA and RNA-Seq analysis were applied to find the key gene network associated with colorectal cancer liver metastasis. Then we performed pathway enrichment analysis on liver metastasis-associated gene set. Immunohistochemistry, *in vitro* and *in vivo* studies were conducted to test expression and function of FOXP3 in CRC tissues and liver metastasis tissues. Non-targeted metabolomics analysis was performed to identify the alteration of FOXP3 expression in metabolites of colorectal cancer liver metastasis. Western blot was performed to confirm changes of matrix metalloproteinase 9MMP9 expression were downstream events of S-adenosyl-methionine (SAM).

Results: We found that FOXP3 and MMP9 exhibited co-expression relationships and affected liver metastasis in CRC. Upregulation of FOXP3 promotes cell migration and invasion in CRC, which suggests a pro-cancer effect. Moreover, metabolomics analysis showed that knockdown of FOXP3 significantly reduced SAM levels, and changes of MMP9 expression were downstream events of SAM, which is concentration-dependent. Besides, The Kyoto Encyclopedia of Genes and Genomes (KEGG) and Western blot analysis confirmed that overexpression of FOXP3 activates the Wnt pathway to promote colon cancer metastasis.

Conclusions: Our results altogether suggested that FOXP3 expression inhibited the SAM cycle to reduce SAMe levels, resulting in altered MMP9 expression and helped CRC liver metastasis.

Keywords: Colorectal carcinoma (CRC); liver metastasis; FOXP3; metabolomics; transcriptome; MMP9

Submitted Mar 30, 2020. Accepted for publication Apr 27, 2020.
doi: 10.21037/atm-20-3287
View this article at: http://dx.doi.org/10.21037/atm-20-3287

Introduction

Colorectal cancer (CRC) tends to be one of the major causes of death from cancer. CRC ranks third among males as the most prevalent cancer, and second among females in the world (1,2). Survival rates for CRC can vary according to a variety of factors, especially the clinical stage. CRC patients' 5-year survival rate is significantly reduced, followed by an increase in Tumor-Node-Metastasis (TNM) staging levels. For example, the 5-year survival rate of patients with localized cancer (stage I) is about 95%, while the 5-year survival rate is about 13% with distant metastasis (stage IV). In CRC, liver is the most common site for distant metastasis. At diagnosis, 25 percent of CRC patients are confirmed to be present with liver metastases (2). The exact mechanism of the CRC liver metastases, however, is still uncertain. To produce successful therapies, therefore, it is important to elucidate the molecular mechanisms and genetic alterations.

FOXP3 is a member of a group of evolutionarily conserved transcriptional regulators (forkhead box proteins) distinguished by a winged-helix DNA-binding domain (3). FOXP3 plays a critical role in the transfer of immune tolerance and the development of the immunosuppressive tumor microenvironment for master regulating the growth and function of regulatory T-cells, notably the CD4+CD25+ subset derived from the thymus (natural Tregs) (4).

An accumulating amount of data has shown that FOXP3 is disrupted in cancer cells. Research has been carried out into the expression of FOXP3 in a variety of human cancer cells (5-8). The majority of studies have indicated that when FOXP3 is expressed, growth benefit is conferred to cancer cells, which correlates with unfavorable prognosis. However, some other reports have suggested the opposite (9,10).

In CRC, Kim *et al.* suggested a poor prognosis has been associated with a higher level of FOXP3 in colon cancer cells (11). Sun *et al.* came to the opposite conclusion, in that FOXP3's high expression was related to a longer overall and disease-free survival rate. The positive rate of expression was significantly associated with the degree of differentiation, depth of infiltration, metastasis of the lymph nodes and staging of pTNM (12). Nonetheless, contradictory events of FOXP3 expression in CRC and the molecular mechanism of regulation of the FOXP3-mediated gene were not fully characterized.

Metabolism dysregulation is a hallmark in cancer cells, being the totality of reactions that produce energy for supporting the cancer cells alive. The essential amino acid methionine is an emergent feature of the cancer metabolism. Methionine is an essential amino acid containing sulfur which, as part of the methionine process, sequentially undergoes catabolism and recycling. In the methionine cycle methionine is transformed into S-adenosyl-methionine (SAM), the fundamental methyl donor. SAM treatment for hepatocellular carcinoma (HCC) induced with different carcinogens and hepatocarcinogenesis protocols in rats can actively prevent tumors from developing (13).

Furthermore, forced evaluation of SAM in human HCC cells was demonstrated to exhibit a suppressive effect *in vivo* tumorigenicity in mice (14). These findings show that SAM has a tumor prevention effect. However, the mechanisms of SAM responsible for the effects of cancer metastases still need to be discussed.

Here, by using clinical correlation, conducting cell- and xenograft-based investigations, and analyzing transcriptomes and metabolomics, we explored FOXP3 activity in CRC liver metastases. We showed the effect of FOXP3 on the prognosis of CRC, elevated FOXP3 expression associated with poor survival in CRC. Overexpression of FOXP3 facilitated MMP9 expression through the SAM cycle to modulate CRC liver metastasis. We present the following article in accordance with the ARRIVE reporting checklist (available at http://dx.doi.org/10.21037/atm-20-3287).

Methods

Patients and variables

We retrospectively searched for fresh frozen tissues of CRC patients with liver metastasis collected from Liaoning Cancer Hospital & Institute. All the patients were diagnosed with primary CRC with synchronous liver metastasis or heterochrony liver metastasis. A precise pathological diagnosis was needed for both primary and metastatic lesions. Simultaneously, data were gathered from the patients' recorded general clinical and comprehensive pathology information. Written informed consent was obtained from each patient, and the the study protocol received approval from the ethics committee of the Liaoning Cancer Hospital & Institute (Approval No.: 20181225).

TCGA cohort and GEO cohort

RNA-seq data of CRC was downloaded from GSE50760. A total of 54 samples were collected, including CRC

tissues, adjacent non-tumorous colorectal tissues, and liver metastasis tissues. The expression profiles of 19,067 coding genes were then measured. The data were preprocessed as follows: the FPKM data was downloaded, and the mean value was chosen to be the initial expression value of the gene for multiple transcripts of the same gene. Pathway enrichment analysis was then carried out through the DAVID (https://david.ncifcrf.gov/) online platform (15). Afterward, weighted co-expression networks were constructed, facilitated by the blockwiseModules function in the WGCNA package (https://labs.genetics.ucla.edu/horvath/CoexpressionNetwork/Rpackages/WGCNA/Tutorials/) on the R platform (https://www.r-project.org/). TCGA-COAD and TCGA-READ transcriptome cohort data were available from the cBioPortal for Cancer Genomics website (http://www.cbioportal.org/) (16).

Cell lines and cultures

Human colorectal carcinoma RKO cells (ATCC, Manassas, VA, USA) were cultured in Dulbecco's Modified Eagle's Medium (DMEM, GenDEPOT) supplemented with 10% fetal bovine serum (GenDEPOT) in a CO_2 incubator at 5% humidity. Human embryonic kidney epithelial cell line 293T was bought from Invitrogen and cultured in RPMI-1640 medium. Cells were transfected with plasmid DNA using Lipofectamine 3000 (Invitrogen, Carlsbad, CA, USA). Cells in the exponential growth phase were used for the assays.

Immunohistochemical (IHC) staining and evaluation

Immunostaining of FOXP3 was carried out with rabbit monoclonal anti-FOXP3 antibody (1:3,000, Cat. ab214, Abcam, USA). Two experienced pathologists independently assessed the staining of a specific protein in one FFPE slide. Staining intensity was scored as follows: 0: no staining; 1: weak; 2: medium; and 3: strong staining. Staining extent was graded from 0 to 4, according to the coverage percentage of immunoreactive tumor cells (0%, 1–25%, 26–50%, 51–75%, 76–100%). The scores of staining intensity and extent were multiplied, and the total IHC score (on a scale of 0 to 12) was calculated. A score of 0 to 3 signified negative staining and a score of 4 to 12 signified positive staining.

Cell invasion assay

Cell invasion was determined by Transwell assay was conducted to determine the cell invasion. The transfected cells were collected and resuspended in serum-free DMEM medium and cultured on the Matrigel-coated upper surface chamber. FBS medium was put in the lower chamber. A cotton swab was used to remove the remaining cells on the upper membrane surface after 24 h incubation. Next, 4% paraformaldehyde was used to fix the cells adhered to the surface of the lower membrane, and 0.1 per cent crystal violet was used for staining. Then, an optical microscope was used to count the cells.

Quantitative real-time PCR

SYBR® Premix Ex Taq™ (Takara, Dalian, China) on Quantstudio™ 12 k Flex Real-time PCR system (Applied Biosystems, Foster City, CA) was used to detect relevant genes. The primer sequences are included in *Table S1*.

Western blot

The anti-N-Cadherin (Cell signaling, 1:2,000), anti-E-Cadherin (Cell Signaling, Danvers, MA, USA, 1:2,000), anti-Vimentin (Abcam, 1:1,000), anti-Snail (Cell signaling, 1:2,000), anti-MMP9 (Cell signaling, 1:2,000), anti-GADPH (Santa Cruz, 1:3,000), anti-c-Myc (Santa Cruz, 1:1,000), and anti-Cyclin D1 (Santa Cruz, 1:1,000), antiFOXP3 (Abcam 1:3,000, Cell signaling 1:2,000) served as the primary antibodies. A 1:3,000–5,000 dilution of the HRP-linked anti-IgG (Santa Cruz) was used as the secondary antibody.

Construction of gene co-expression network between DEGs and DELs

A scale-free co-expression network for the hub DEGs and DELs was constructed with the WGCNA R package. Gene expression similarity matrix was formed by calculating the Pearson correlation coefficient between two genes, which was then transformed into adjacency matrix (a threshold power of β=5), and subsequently into a topological matrix. The extent of the relationship between genes/lncRNAs was determined by topological overlap measure (TOM). The overall level of gene expression within the module was indicated through the calculation of module eigengene (ME) to define the first principal component for a module. The key module can be found by calculating Pearson correlation coefficients between ME in each module and sample traits. Hub genes which met the criteria of having a module

Table 1 FOXP3 expression associated with clinical-pathological characteristics

Characteristics	No. of cases	Percent %	P value
Age (years)			0.831
≥60	18	62.07	
<60	11	37.93	
Gender			0.877
Male	23	79.31	
Female	6	20.69	
Grade			0.051
G1	6	20.69	
G2	–	–	
G3	23	79.31	
Diameter (cm)			0.179
≥5	5	17.24	
<5	24	82.76	
T stage			0.02
T1–2	7	24.14	
T3	11	37.93	
T4	11	37.93	
Liver metastasis			0.042
Heterochrony liver metastasis	22	75.86	
Synchronous liver metastasis	7	24.14	

membership (MM) value of more than 0.9 were chosen.

SAM detection

The Bridge-It® S-Adenosyl Methionine (SAM) Fluorescence Assay Kit was used to assess the SAMe levels in line with the manufacturer's protocol. The cells that stably expressed scrambled shRNA or FOXP3-shRNA were used to transiently express empty vector or FOXP3-overexpressing plasmid.

DNA methyltransferase (DNMT) inhibition experiment

DNMT inhibitor, SGI-1027, was employed to inhibit DNMT activity. At 24 or 48 h after transfection, 2 μM of this compound was supplemented in culture medium for 24 h. Protein extraction and total RNA isolation were then conducted.

Statistical analysis

Chi-square test (Fisher's exact test) was used to analyze categorical variables. Two-sided *t*-test was used to compare continuous variables, and ANOVA analysis was used for multiple sets of continuous variables. Correlation between continuous variables was summarized using Spearman's rank test. All statistical analyses were performed using R version 3.5.3. Statistical significance was represented by $P<0.05$.

Results

Clinicopathological characteristics of the cohorts

A total of 29 CRC and liver metastasis samples with FOXP3 expression data across patient characteristics were analyzed in this study. Patients with elevated FOXP3 expression in CRC tissue were significantly correlated with T stage (P=0.02) and synchronous liver metastasis (P=0.042) (*Table 1*). Chi-square test revealed that patients with high FOXP3 expression are prone to progress to a more advanced stage and synchronous liver metastasis than those with low FOXP3 expression.

FOXP3 is highly expressed in CRC and associated with worse clinical outcome

To establish if FOXP3 is expressed in CRC, and to explore if it has any correlation with patient outcome, we carried out immunohistochemistry (IHC) on CRC and colorectal cancer liver metastasis (CRCLM) tissues. FOXP3 immunostaining was seen in CRC and CRCLM cells (*Figure 1*). FOXP3 expression showed diffuse staining in both the cytoplasm and the nucleus. Statistically, in comparison with normal adjacent tissues, elevated FOXP3 was significantly expressed in cancerous tissues and metastatic liver tissues ($P<0.001$). DEGs analysis was performed in TCGA-COAD and TCGA-READ to confirm this finding. *Figure 2* gives the verification results that FOXP3 is highly expressed in cancer than normal adjacent tissues in the TCGA cohort ($P<0.05$).

Ectopic expression of FOXP3 facilitates proliferation and migration of CRC cells in vitro and in vivo

To measure the role of ectopic expression of FOXP3 on cancer cells, FOXP3 lentivirus was transfected into CRC

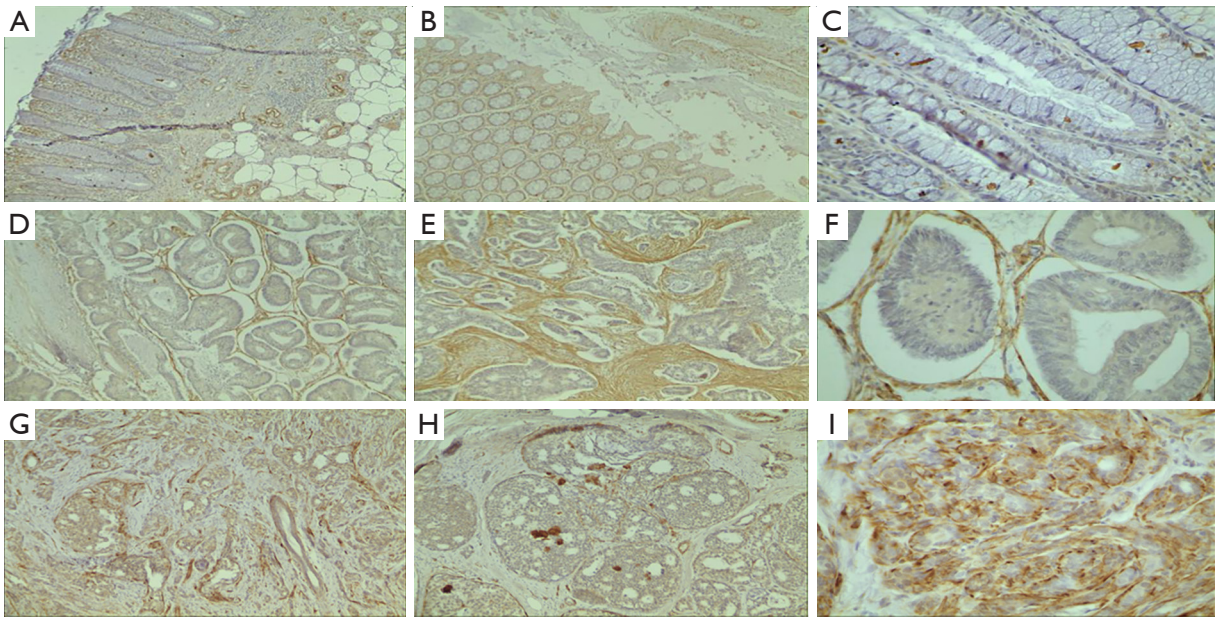

Figure 1 Immunohistochemical staining of FOXP3. (A,B) Immunohistochemical staining of FOXP3 in colorectal normal adjacent tissues, magnification 100×. (C) Magnification 400×. (D,E) Primary cancer tissues, magnification 100×. (F) Magnification 400×. (G,H) Liver metastatic tissues, magnification 100×. (I) Magnification 400×.

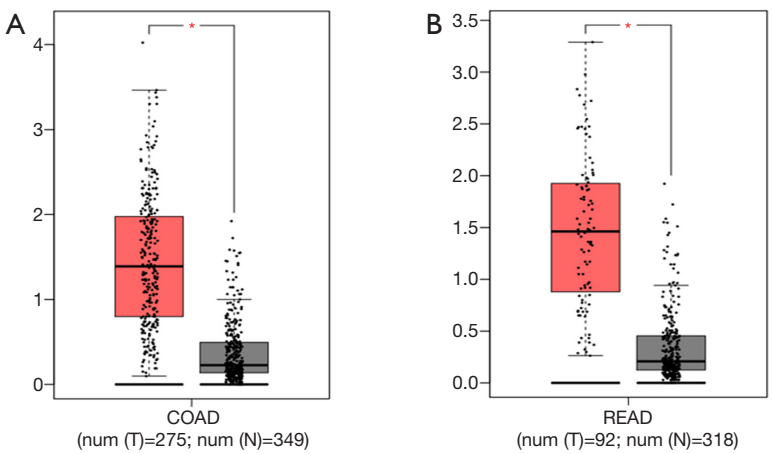

Figure 2 FOXP3 is upregulated in colorectal carcinoma patients. (A) GEPIA expression analysis of FOXP3 in human colon carcinoma patients. Orange box: 275 colon carcinoma patients; blue box: 349 healthy donors. (B) GEPIA expression analysis of FOXP3 in human rectal carcinoma patients. Orange box: 92 rectal carcinoma patients; blue box: 318 healthy donors. *, P<0.05.

cell lines (RKO and HT-29), and Western blot was carried out to validate FOXP3 expression (*Figure 3A*). We found that overexpression of FOXP3 promotes cell growth *in vitro* (*Figure 3B*). Besides, elevated expression of FOXP3 significantly increases cell viability in the invasion and migration of RKO cells (*Figure 3C,D,E,F*).

Because cell growth is promoted by FOXP3 *in vitro*, we next the contribution of FOXP3 in CRC cell growth *in vivo*. After 18 days of inoculation , the average tumor volume in the overexpression FOXP3-infected group was observed to be 2.6-fold more extensive than that of control group. The tumors of the RKO-FOXP3 and RKO-Control groups of nude mice are shown in *Figure 4A* and *B*. Overall, these results illustrated that FOXP3 performs distinct oncogene

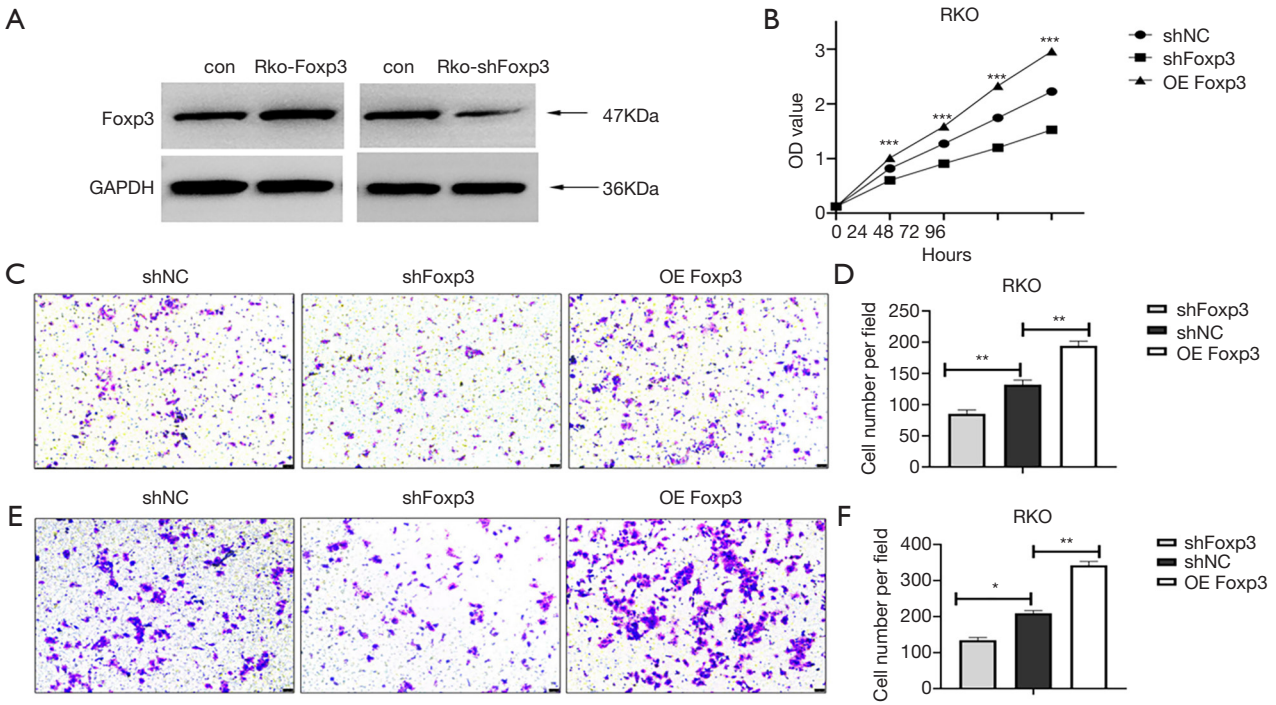

Figure 3 Functional properties of the FOXP3 *in vitro*. (A) FOXP3 lentivirus was transfected or knocked out CRC cell lines, and FOXP3 expression was assessed by Western blot; (B) the subcutaneous tumor cell growth curve of overexpression FOXP3 and shFOXP3 was compared with the control cells. Enhanced tumor growth was exhibited in the OE-FOXP3 group in comparison with the control group (P<0.05); (C,D) FOXP3 knockdown inhibited CRC cell's invasive capability as compared to the effect of the negative control, magnification 100×; (E,F) FOXP3 knockdown inhibited CRC cell migration capability as compared to the effect of the negative control, magnification 100×. *, P<0.05; **, P<0.01; ***, P<0.001. All data are the mean ± SD. CRC, colorectal cancer.

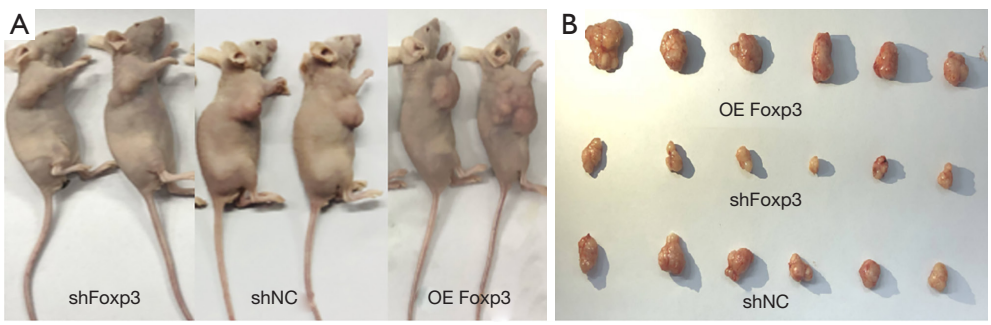

Figure 4 Tumor samples after stable transplantation of different groups of colon carcinoma cells in nude mice. (A) Images of the different tumor samples following stable of different groups of cells; (B) tumor size after stable transplantation in nude mice.

functions in CRC.

Weighted gene co-expression network analysis of differential genes

Since FOXP3 displays metastasis-related properties, including cell proliferation and migration in CRC, we intended to find a series of combined action genes that promote liver metastasis from a whole transcriptome perspective.

WGCNA was exploited to conduct closely co-expressed high-variant genes (HVGs) into co-expression gene sets. A total of 8,844 HVGs were regarded as the candidate genes

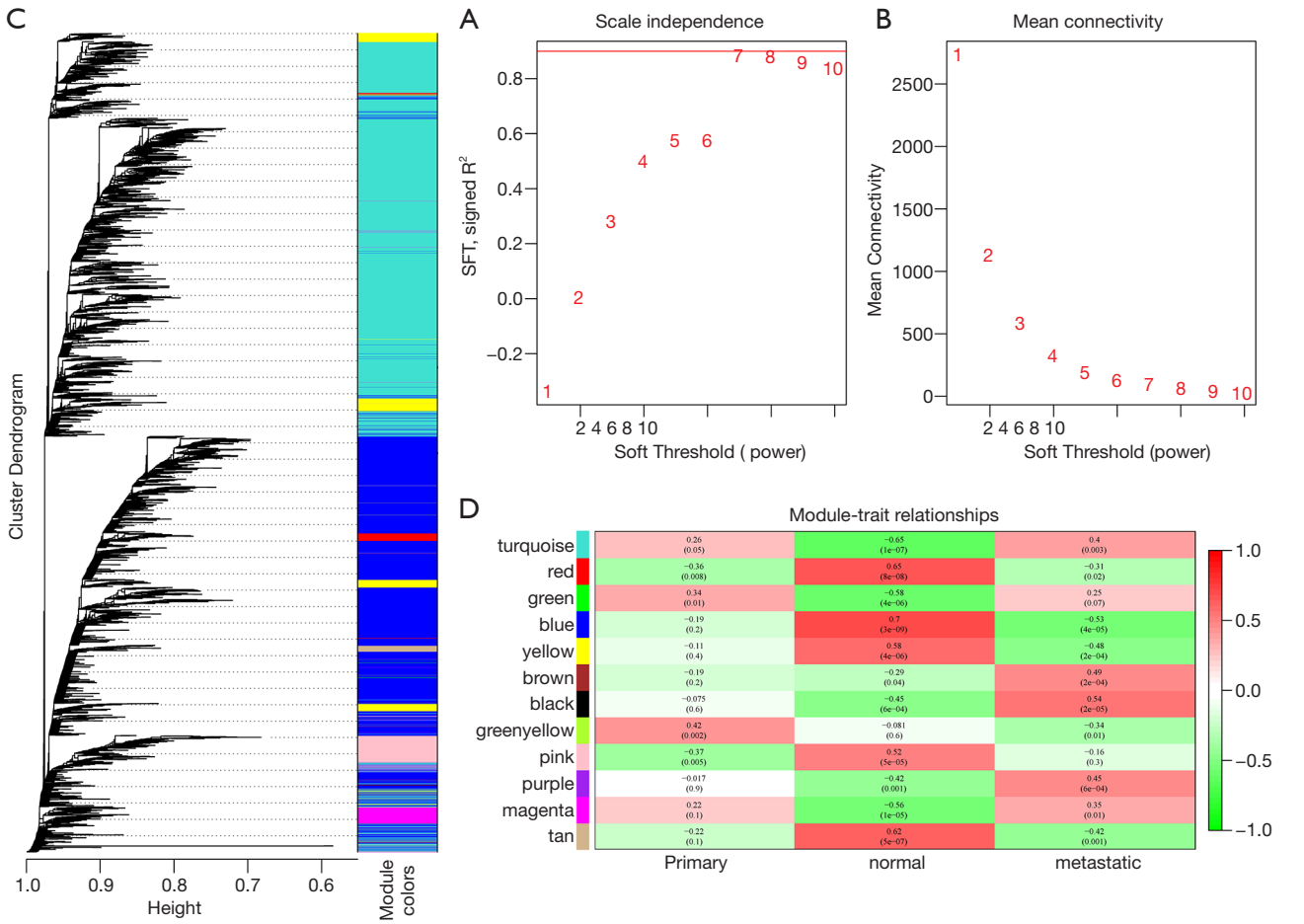

Figure 5 WGCNA network and module detection. (A) Selection of the soft-thresholding powers. The left panel shows the scale-free fit index versus the soft-thresholding power; (B) the right panel displays the mean connectivity versus the soft-thresholding power. Power 7 was chosen because the fit index curve flattened out upon reaching a high value (>0.9); (C) cluster dendrogram and module assignment for modules from WGCNA. Genes cluster dendrogram drawn using a dissimilarity measure (1-TOM). The colored horizontal bar below the dendrogram represent the modules. A total of 8,844 genes were assigned to one of 12 modules including the gray module; (D) each column corresponds to a clinical feature (primary tissues, normal tissues, or metastatic tissues) and each row to an eigengene module. Each cell contains the corresponding correlation on the first line and the P value on the second line. The table is color-coded by correlation according to the color legend. The gray module included all the genes that could not be clustered.

and clustered by average linkage hierarchical clustering analysis by transforming adjacency matrix into TOM, and each network module was set with a minimum of 30 genes based on Dynamic Tree Cut standard (*Figure 5A,B*). Twelve new modules were generated from the calculated eigengenes of each module (*Figure 5C*). The genes unable to be clustered into other modules were clustered into the gray modules.

Pearson's correlation coefficient measured the relationship between each element and the clinical traits (*Figure 5D*). Genes in yellow, black, brown, magenta, green, blue, and red modules were related to healthy tissues, while genes in green, yellow, purple, pink, and turquoise modules were related to colorectal carcinoma tissues. Meanwhile, the black module was significantly related to the liver metastasis characteristic. Genes included FOXP3 in the black modules are listed in *Table S2*.

We conducted a KEGG pathway enrichment analysis to reveal the general functional features of the liver metastasis-associated gene set. Notably, pathway enriches in the

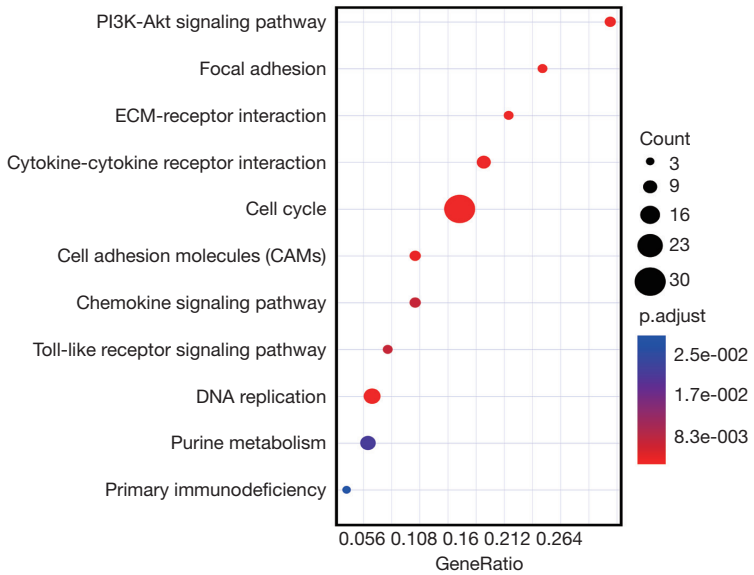

Figure 6 KEGG pathway enrichment analyses for genes in the black module.

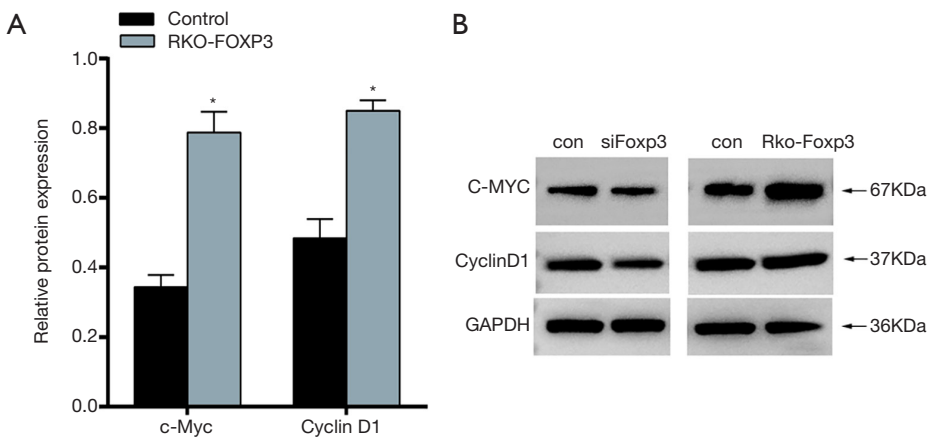

Figure 7 FOXP3 upregulated protein expression of c-Myc and Cyclin D1 in RKO cells. (A) FOXP3 upregulated mRNA expression of c-Myc and Cyclin D1 in RKO cells, while silencing FOXP3 downregulated mRNA expression of c-Myc and Cyclin D1 in RKO cells; (B) over expression of FOXP3 upregulated protein expression of c-Myc and Cyclin D1 in RKO cells, while silencing FOXP3 downregulated protein expression of c-Myc and Cyclin D1 in RKO cells. *, P<0.05.

process of promoting tumorigenicity, including cell cycle, DNA replication, cell adhesion molecules (CAMs), and chemokine signaling pathway (17,18) (*Figure 6*).

Ectopic expression of FOXP3 activates Wnt/β-catenin pathway in CRC cells

MMP9, Cyclin D1, c-Myc were co-expressed in the black module, which was correlated with CRCLM in transcriptome analysis, and were marker genes in Wnt/β-catenin signaling (19). We further examined the expression of c-Myc and Cyclin D1. Both qPCR (*Figure 7A*) and Western blot (*Figure 7B*) revealed the expression of c-Myc and Cylin D1 to be elevated when FOXP3 was ectopically expressed, which indicated that FOXP3 overexpression stimulates the Wnt/β-catenin pathway in CRC cells.

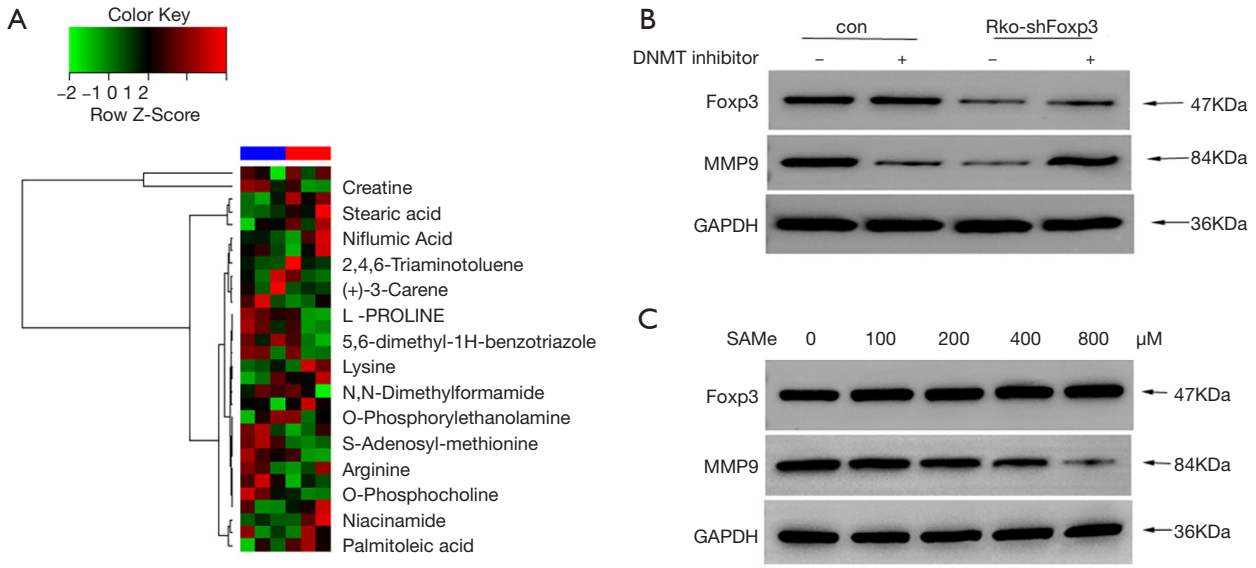

Figure 8 MMP9 expression mediated by FOXP3 is through the metabolism of SAM. (A) Metabolomics analysis showed silence of FOXP3 in colorectal cancer cells significantly increases S-adenosyl-methionine levels; (B) western blot analysis of expression of MMP9 pre-treated with or without DNMT inhibitor; (C) western blot analysis expression of MMP9 pre-treated with SAM in wrote down concentrations.

FOXP3 upregulated MMP9 expression through methylthioadenosine (MTA) cycle to modulate colorectal carcinoma metastases

Metastatic colonization formation has been seen to be a significant rate-limiting step during metastatic liver growth (20). This selective pressure may be due in part to the hypoxic microenvironment as well as substantial metabolic activity (21). Therefore, we conducted metabolomics to perform the effect of FOXP3 on tumor metabolism.

Many methionine-related elements of metabolism are linked to cancer. The methionine cycle sees the conversion of methionine to the universal methyl donor SAM, which is converted to S-adenosyl-homocysteine (SAH) after the donation of its methyl group. Through non-target metabolomics analysis, we found that SAM was significantly increased in the siFOXP3 group (*Figure 8A*). One role methionine plays in controlling cancer-associated phenotypes is mediating gene expression through epigenetic mechanisms. These results suggest that over the SAM cycle, FOXP3 promotes liver metastasis in CRC.

We knocked down FOXP3 via siRNA transfection strategy to shine a light on the role of FOXP3 in the modulation of these co-expression hub genes. The level of mRNA expression of the 10 selected hub genes (*Figure S1*) was then calculated using qRT-PCR. Results showed that reduction in the expression of FOXP3 significantly reduced the expression of MMP9 more than two-fold (*Figure 8B*). The matrix metalloproteinases-9, MMP-9, is a significant protease, which is able to regulate ECM remodeling by cleaving many extracellular matrix (ECM) proteins and performs a pivotal task in cancer cell invasion and tumor metastasis. To confirm the impact of FOXP3 on MMP9 expression, western blot analysis, and RT-qPCR were performed in FOXP3 stably expressing cells. The protein and mRNA levels of MMP9 were observed to be markedly increased in cells exhibiting FOXP3 overexpression, as shown in *Figure 8C*. Conversely, knockdown of FOXP3 significantly reduced MMP9 protein and mRNA expression.

Next, we analyzed whether the downregulation of MMP9 was a downstream event of the SAM cycle according to the results in *Figure 8A*. As expected, the expression of MMP9 was significantly higher under the supplementation of DNMT inhibitor in cells with FOXP3 overexpression. Also, we analyzed the MMP9 expression level following SAM treatment at various concentrations for 72 h. Accordingly, we noticed a decrease in the MMP9 protein level in a SAM dose-dependent manner. These findings altogether confirmed the hypothesis that FOXP3 negatively regulates SAM and therefore reduced MMP9 promoter methylation to induce its expression.

Discussion

The significant finding from this study is that we indicated FOXP3 acts as a potent oncogene in CRC liver metastasis. Overexpression of FOXP3 enhanced CRC cells with metastatic behavior via activating the Wnt/β-catenin signaling pathway. This resulted in a hyperactivation condition. which is a core characteristic of CRC development. FOXP3-mediated S-adenosylmethionine regulated MMP9 promoter demethylation, upregulating expression of MMP9, which has been widely found to relate to the invasion, metastasis, and angiogenesis pathology of cancers. High FOXP3 expression was significantly associated with poor outcomes in CRC patients. Collectively, our data showed that a high level of FOXP3 expression in cancer cells plays a pivotal role in propelling CRC liver metastasis and decreasing patient survival. It paves a novel way for FOXP3 expression to be able to influence the pathogenesis of CRC liver metastasis via interference with S-adenosylmethionine metabolism.

It is well known that FOXP3 is a specific marker of regulatory T cells (Tregs), and that performs a vital task in the differentiation of Tregs to mediate tumor immune escape (17,22). However, recently its expression has been shown in distinct types of human tumor cells. FOXP3 exhibited paradoxical roles in different types of tumors. Li *et al.* demonstrated that FOXP3 suppresses angiogenesis of breast cancer by downregulating the expression of VEGF (18). Guo *et al.* revealed that the expression of FOXP3 was correlated with the grade of gastric lesion, indicating that FOXP3 may have an essential function in gastric cancer formation, development and prognosis (23). Shi *et al.* suggested that FOXP3 has a suppressive effect on the progression of HCC tumors via the transforming growth factor-beta (TGF-β)/Smad2/3 signaling pathway, which presents FOXP3 as a factor in the prognosis of and a novel target for the optimal treatment of HCC (24).

On the contrary, Tang *et al.* showed that there is a positive correlation between FOXP3 and vascular endothelial growth factor-C (VEGF-C) expression and lymphangiogenesis in cervical cancer (25). Mechanistically, Gao *et al.* found that nuclear Galectin-1 (Gal-1) interferes with the binding process between FOXP3 and DNA through its interaction with FOXP3's FKH domain, which may the possible mechanism behind the loss of the tumor-suppressive properties of FOXP3 in wild-type FOXP3-positive breast cancer (26). In this study, data analysis of our cohort and CRC cells supported our hypothesis; the high expression of FOXP3 detected in tumor tissues from CRC patients led to the activation of the Wnt signaling pathway and decreased overall survival.

KEGG analysis illustrated that prostate cancer samples were enriched with meiotic recombination 11 (MRE11), which is involved in the most significant pathways, including the mitotic spindle, ultraviolet response, and TGF-β signaling pathways. Of the Wnt signaling pathways, the established Wnt/β-catenin pathway has been investigated most extensively. In the established pathway, when there are adequate levels of β-catenin, a fraction of cytoplasmic β-catenin migrates to the nucleus to interact with the LEF-1/T-cell factor (TCF) family transcription factors. As a consequence, these transcription factors stimulate the activation of oncogenes involved in EMT, survival, angiogenesis motility, and invasion, including c-Myc, VEGF, monocyte chemo-attractant protein 1 (CCL2), snail, slug, vimentin, and metalloproteinases (27-30). To this end, FOXP3 was chosen for further study of its potent role in driving metastasis, considering its recognized role in promoting CRC cell migration and invasion.

The relationship between FOXP3 and CRC liver metastasis has seldom been reported, although notably, MRE11 has been confirmed to support a reduced overall survival rate and is believed to be highly expressed in tissues from CRC tumors and liver metastasis.

Metabolomics analysis of CRC cells revealed that the metastasis promotion effect by FOXP3 was mediated through the SAM cycle. Following our results, Luo *et al.* reported that SAM could effectively exhibit an inhibitive effect on tumor cell growth via the reversal of DNA hypomethylation on oncogene promoters, leading to the downregulation of their expression. As it has no effect on the expression of P16 and other tumor suppressor genes, SAM could potentially be applied in cancer therapy (31). This was suggested in the study of Luo *et al.* (31). Previous studies also found that SAM acts as a regulator of apoptosis and autophagy in MCF-7 breast cancer cells via the microRNA-specific modulation (32). On the other hand, Shi *et al.* reveal that SAM presents as evidence of tumor suppression, especially on primary osteosarcoma, but it lacks positive effects on metastatic osteosarcoma (33). All these studies prove that the SAM cycle plays a significant role in tumor growth and development. Further, Greenberg *et al.* demonstrate that plasma levels of SAM are significantly elevated in lung cancer patients and, in combination with chest CT, may serve as a helpful tool for the early diagnosis of lung cancer (34).

In our study, FOXP3 inhibition was shown to suppress the expression of MMP9, which was characteristic of a downstream event of the SAM cycle. It has been reported that MMP9 can be an essential driver of tumor growth and metastasis in many types of tumors. Bing Xia *et al.* revealed circular RNA derived from MMP9 facilitates oral squamous cell carcinoma metastasis through regulation of MMP9 mRNA stability (35). Similarly, Diosmetin was found to influence the inhibition of SK-HEP-1 and MHcc97H cell metastasis through the downregulation of MMP-2/9 expression via the PKC/MAPK/MMP pathways (36). Moreover, Chen *et al.* reported that G-protein-coupled receptor kinase-interacting protein 1 can facilitate tumor progression via the activation of ERK/MMP9 signaling in hepatocellular carcinoma (37). We recognized that FOXP3 affects MMP9 expression is in a SAM-dependent way. SAM can effectively inhibit the tumor cell growth via the reversal of the DNA hypomethylation on oncogene promoters, without influencing the expression of the tumor suppressor genes. These results suggest that SAM could potentially be an option for cancer treatment.

At the same time, our study has limitations as follows. Firstly, this study is a retrospective small sample study. Besides, the revelation of detailed mechanism between FOXP3 and metastasis of CRC as well as specific relation of SAM and MMP9 need further experiments to confirm.

In conclusion, our study reveals the relationship that increased FOXP3 expression has with liver metastasis and poor survival in CRC patients. These data indicate that FOXP3 may function as an oncogene and that it holds promise as a biomarker for CRC patients with liver metastasis. More validation cohorts and further elucidation are needed so that all of the values of FOXP3 in cancer cells and its clinical application for CRC liver metastasis can be established.

Acknowledgments

Funding: Science and Technology Planning Project of Shenyang (No. 191124088); Science and Technology Planning Project of Liaoning Province of China (No. 201800449); Natural Science Foundation of Liaoning Province (No. 20180550781). Scientific research foundation for the introduction of talents, Liaoning Cancer Hospital & Institute (No. Z1702).

Footnote

Reporting Checklist: The authors have completed the ARRIVE reporting checklist. Available at http://dx.doi.org/10.21037/atm-20-3287

Data Sharing Statement: Available at http://dx.doi.org/10.21037/atm-20-3287

Conflicts of Interest: Both authors have completed the ICMJE uniform disclosure form (available at http://dx.doi.org/10.21037/atm-20-3287). The authors have no conflicts of interest to declare.

Ethical Statement: The authors are accountable for all aspects of the work in ensuring that questions related to the accuracy or integrity of any part of the work are appropriately investigated and resolved. Written informed consent was obtained from each patient, and the study protocol received approval from the Ethics Committee of the Liaoning Cancer Hospital & Institute (Approval No.: 20181225).

References

1. Ferlay J, Soerjomataram I, Dikshit R, et al. Cancer incidence and mortality worldwide: sources, methods and major patterns in GLOBOCAN 2012. Int J Cancer 2015;136:E359-86.
2. Henry JT, Johnson B. Current and evolving biomarkers for precision oncology in the management of metastatic colorectal cancer. Chin Clin Oncol 2019;8:49.
3. Chen X, Yan S, Zhao H, et al. The safety and feasibility of a single incision in simultaneous resection for patients with colorectal cancer liver metastases. Ann Transl Med 2019;7:547.
4. Lal G, Bromberg JS. Epigenetic mechanisms of regulation of Foxp3 expression. Blood 2009;114:3727-35.
5. Hinz S, Pagerols-Raluy L, Oberg HH, et al. Foxp3 expression in pancreatic carcinoma cells as a novel mechanism of immune evasion in cancer. Cancer Res

2007;67:8344-50.
6. Wang L, Liu R, Li W, et al. Somatic single hits inactivate the X-linked tumor suppressor FOXP3 in the prostate. Cancer Cell 2009;16:336-46.
7. Weller P, Bankfalvi A, Gu X, et al. The role of tumour FoxP3 as prognostic marker in different subtypes of head and neck cancer. Eur J Cancer 2014;50:1291-300.
8. Zhang HY, Sun H. Up-regulation of Foxp3 inhibits cell proliferation, migration and invasion in epithelial ovarian cancer. Cancer Lett 2010;287:91-7.
9. Ma GF, Miao Q, Liu YM, et al. High FoxP3 expression in tumour cells predicts better survival in gastric cancer and its role in tumour microenvironment. Br J Cancer 2014;110:1552-60.
10. Suh JH, Won KY, Kim GY, et al. Expression of tumoral FOXP3 in gastric adenocarcinoma is associated with favorable clinicopathological variables and related with Hippo pathway. Int J Clin Exp Pathol 2015;8:14608-18.
11. Kim M, Grimmig T, Grimm M, et al. Expression of Foxp3 in colorectal cancer but not in Treg cells correlates with disease progression in patients with colorectal cancer. PLoS One 2013;8:e53630.
12. Sun X, Feng Z, Wang Y, et al. Expression of Foxp3 and its prognostic significance in colorectal cancer. Int J Immunopathol Pharmacol 2017;30:201-6.
13. Pascale RM, Simile MM, De Miglio MR, et al. Chemoprevention of hepatocarcino-genesis: S-adenosyl-L-methionine. Alcohol 2002;27:193-8.
14. Li J, Ramani K, Sun Z, et al. Forced expression of methionine adenosyltransferase 1A in human hepatoma cells suppresses in vivo tumorigenicity in mice. Am J Pathol 2010;176:2456-66.
15. Skrlj B, Kunej T. Computational identification of non-synonymous polymorphisms within regions corresponding to protein interaction sites. Comput Biol Med 2016;79:30-35.
16. Gao J, Aksoy BA, Dogrusoz U, et al. Integrative analysis of complex cancer genomics and clinical profiles using the cBioPortal. Sci Signal 2013;6:pl1.
17. Plitas G, Rudensky AY. Regulatory T Cells: Differentiation and Function. Cancer Immunol Res 2016;4:721-5.
18. Li X, Gao Y, Li J, et al. FOXP3 inhibits angiogenesis by downregulating VEGF in breast cancer. Cell Death Dis 2018;9:744.
19. Veeman MT, Axelrod JD, Moon RT. A second canon. Functions and mechanisms of be-ta-catenin-independent Wnt signaling. Dev Cell 2003;5:367-77.
20. Kauffman EC, Robinson VL, Stadler WM, et al. Metastasis sup-pression: the evolving role of metastasis suppressor genes for regulating cancer cell growth at the secondary site. J Urol 2003;169:1122-33.
21. Bristow RG, Hill RP. Hypoxia and metabolism. Hypoxia, DNA repair and genetic in-stability. Nat Rev Cancer 2008;8:180-92.
22. Mohr A, Atif M, Balderas R, et al. The role of FOXP3+ regulatory T cells in human autoimmune and inflammatory diseases. Clin Exp Immunol 2019;197:24-35.
23. Guo G, He Z, Shi Z. Correlation between FOXP3 expression and gastric cancer. Oncol Lett 2016;12:1554-8.
24. Shi JY, Ma LJ, Zhang JW, et al. FOXP3 Is a HCC suppressor gene and Acts through regulating the TGF-β/Smad2/3 signaling pathway. BMC Cancer 2017;17:648.
25. Tang J, Yang Z, Wang Z, et al. Foxp3 is correlated with VEGF-C expression and lymphangiogenesis in cervical cancer. World J Surg Oncol 2017;15:173.
26. Gao Y, Li X, Shu Z, et al. Nuclear galectin-1-FOXP3 interaction dampens the tumor-suppressive properties of FOXP3 in breast cancer. Cell Death Dis 2018;9:416.
27. Clevers H. Wnt/β-catenin signaling in development and disease. Cell 2006;127:469-80.
28. Wang N, Wang ZY, Wang Y, et al. Dietary compound isoliquiritigenin prevents mammary carcinogenesis by inhibiting breast cancer stem cells through WIF1 de-methylation. Oncotarget 2015;6:9854-76.
29. Kwon OJ, Valdez JM, Zhang L, et al. Increased Notch signal-ling inhibits anoikis and stimulates proliferation of prostate luminal epithelial cells. Nat Commun 2014;5:4416.
30. Przybylo JA, Radisky DC. Matrix metalloproteinase-induced epithelial-mesenchymal transition: tumor progression at Snail's pace. Int J Biochem Cell Biol 2007;39:1082-8.
31. Luo J, Li YN, Wang F, et al. S-adenosylmethionine inhibits the growth of cancer cells by reversing the hypomethylation status of c-myc and H-ras in human gastric cancer and colon cancer. Int J Biol Sci 2010;6:784-95.
32. Ilisso CP, Delle Cave D, Mosca L, et al. S-Adenosylmethionine regulates apoptosis and autophagy in MCF-7 breast cancer cells through the modulation of specific microRNAs. Cancer Cell Int 2018;18:197.
33. Shi H, Mu WD, Zhang B, et al. Potential role of S-adenosylmethionine in osteosarcoma development. Onco Targets Ther 2016;9:3653-9.
34. Greenberg AK, Rimal B, Felner K, et al. S-adenosylmethionine as a biomarker for the early

detection of lung cancer. Chest 2007;132:1247-52.
35. Xia B, Hong T, He X, A circular RNA derived from MMP9 facilitates oral squamous cell carcinoma metastasis through regulation of MMP9 mRNA stability. Cell Transplant 2019;28:1614-23.
36. Liu J, Wen X, Liu B, et al. Diosmetin inhibits the metastasis of hepatocellular carcinoma cells by downregulating the expression levels of MMP-2 and MMP-9. Mol Med Rep 2016;13:2401-8.
37. Chen J, Yang P, Yang J, et al. GIT1 is a novel prognostic biomarker and facilitates tumor progression via activating ERK/MMP9 signaling in hepatocellular carcinoma. Onco Targets Ther 2015;8:3731-42.

Cite this article as: Wang Z, Zhang J. FOXP3 promotes colorectal carcinoma liver metastases by evaluating MMP9 expression via regulating S-adenosylmethionine metabolism. Ann Transl Med 2020;8(9):592. doi: 10.21037/atm-20-3287

Supplementary

Table S1 Primer sequence used for RT-PCR

Gene	Primer sense	Primer anti-sense
GAPDH	5'-TTGTGGAAGGGCTCATGACC-3'	5'-TCTTCTGGGTGGCAGTGATG-3'
FOXP3	5'-GAGAAGCTGAGTGCCATGCA-3'	5'-GGTCAGTGCCATTTTCCCAG-3'
MMP-9	5'-AAAACCTCCAACCTCACGGA-3'	5'-GCGGT-ACAAGTATGCCTCTGC-3'
C-MYC	5'-TTTGTCTATTTGGGGACAGTGTT-3'	5'-CATCGTCGTGGCTGTCTG-3'
Cyclin D1	5'-GCGGAGGAGAACAAACAGAT-3'	5'-GAGGGCGGATTGGAAATGA-3'

Table S2 Genes included FOXP3 in the black modules

Gene	Module
LILRB4	Black
RPLP0P2	Black
CCL2	Black
LPGAT1	Black
STON2	Black
C19orf57	Black
GJB3	Black
MSL3	Black
NPC1	Black
PLK3	Black
CHRNA6	Black
CXCL11	Black
TM4SF1	Black
KCF2	Black
FCGR1B	Black
TACSTD2	Black
POU3F1	Black
SPRED3	Black
FCGR2B	Black
STC1	Black
SLCO1B7	Black
C3AR1	Black
SERPINE1	Black
FCGR1A	Black
KRT6A	Black
LOC100505839	Black
SIGLEC9	Black
CLDN2	Black
STAT1	Black
ITGB2	Black
C2orf68	Black
SLA	Black
RAB42	Black
CD86	Black
VSIG4	Black
LILRA6	Black
IP6K2	Black
ZNF812	Black
PRKCZ	Black
LOC100287314	Black
RECQL	Black
ITGAV	Black
STX11	Black
CHST11	Black
ZNF365	Black
1-Mar	Black
LILRB3	Black
ATP8F1	Black
ETV5	Black
MAP3K8	Black
KRT5	Black
MMP9	Black
PSAP	Black
MAFB	Black
DUSP4	Black
CCR1	Black
LIMS1	Black
GSDMC	Black
ITGAM	Black
MFI2	Black
DRAM1	Black
FRMD5	Black
TMEM219	Black
FAM98C	Black
DCBLD2	Black
CACFD1	Black
ZNF697	Black
CEP170	Black
SPATC1	Black
IGFL2	Black
NR2F6	Black
SLC39A5	Black
GPR84	Black
FGR	Black
PTCRA	Black
LAMC2	Black
OSCAR	Black
SIRPA	Black
CD68	Black
CMTM7	Black
LINC00570	Black
AMPD3	Black
NLRC4	Black
CLEC7A	Black
LOC100289019	Black
HAVCR2	Black
ARL4C	Black
GPR137B	Black
GPR97	Black
FOXC1	Black
CSF3R	Black
CD84	Black
SLC11A1	Black
TM4SF19	Black
RAET1L	Black
CARD6	Black
CYP27B1	Black
CCL4	Black
CD83	Black
SHD	Black
SCIMP	Black
APOL1	Black
ACSL4	Black
TNFSF13B	Black
MRC1	Black
CRISP3	Black
ZFAND2B	Black
GPNMB	Black
MEPE	Black
LHFPL3	Black
UIF	Black
CEP170P1	Black
RXFP3	Black
ADRBK2	Black
OLR1	Black
FCGR2A	Black
C4orf38	Black
APOBR	Black
LEMD1	Black
RELT	Black
FCGR3B	Black
COBL	Black
CHSY1	Black
C12orf59	Black
SIGLEC7	Black
PIK3R5	Black
SLC38A6	Black
DGAT1	Black
MSC	Black
DUSP9	Black
NDUFS3	Black
SIRPB1	Black
SIRPD	Black
CNPPD1	Black
CDC27	Black
LOC644242	Black
LPCAT1	Black
LOC653786	Black
COX8A	Black
DFNA5	Black
TLR4	Black
LRRC25	Black
FOXP3	Black
CCL18	Black
St3GC2	Black
MC4R1	Black
ALOX5AP	Black
PPP1R3E	Black
BCAT1	Black
TPRN	Black
EDARADD	Black
KCNJ5	Black
C19orf59	Black
SIGLEC5	Black
PILRA	Black
C11orf2	Black
NLRP12	Black
EFNA2	Black
COL22A1	Black
CLEC6A	Black
PSTPIP2	Black
SLC39A6	Black
F2R	Black
MAZ	Black
HDHD3	Black
SPHK1	Black
IFI30	Black
CD72	Black
CXCR4	Black
GM2A	Black
NALCN-AS1	Black
MNDA	Black
XRN1	Black
LOC339874	Black
CCL4L1	Black
ALOX15B	Black
SLC46A2	Black
CYP2R1	Black
TIMP1	Black
FCGR1C	Black
PLEKHN1	Black
PI4K2A	Black
CCDC115	Black
SPP1	Black
BTF3L4	Black

Table S2 (*continued*)

Table S2 (*continued*)

Gene	Module
CCDC102B	Black
RNF41	Black
ADAM9	Black
PLAUR	Black
HTRA4	Black
HS3ST2	Black
CSF2RA	Black
C2030C	Black
C12orf70	Black
SLC13A2	Black
C2030E	Black
P2RX7	Black
CD33	Black
PLA2G7	Black
RNF115	Black
ECSIT	Black
NPL	Black
OR7E14P	Black
TNFAIP6	Black
RARB	Black
YOD1	Black
C1QA	Black
TLR2	Black
LOC100505702	Black
TDRD6	Black
C11orf45	Black
C12orf5	Black
MMP7	Black
C1orf162	Black
NUDT22	Black
MREG	Black
SLC16A6	Black
GRIK1-AS2	Black
GJB4	Black
TNFSF18	Black
IRF5	Black
MMP15	Black
IGSF6	Black
HS2ST1	Black
GNA15	Black
GNS	Black
NRD1	Black
LILRA5	Black
LRIT2	Black
SLC7A7	Black
CD163	Black
C1QC	Black
KIRT1.1	Black
KEL	Black
DSE	Black
CLEC5A	Black
PAEP	Black
CYBB	Black
OSM	Black
TYROBP	Black
LINC00256B	Black
TFEC	Black
KIAA1024	Black
SPOCD1	Black
C7orf59	Black
POSTN	Black
IL21R	Black
HCK	Black
EMR2	Black
ARID5A	Black
FUT6	Black
CMAS	Black
LST1	Black
SPI1	Black
B4GALT6	Black
NDUFA1	Black
KLC3	Black
C2030A	Black
DOK4	Black
BTBD11	Black
EMR3	Black
CEACAM4	Black
NAA60	Black
ENTHD1	Black
SLC2A6	Black
CXCR2	Black
TREM2	Black
TNF	Black
PPP1CA	Black
PLA2G6	Black
SNAPC1	Black
SLC41A1	Black
LY86	Black
PITPNC1	Black
GFER	Black
SPR	Black
CLEC4E	Black
DNAJC5B	Black
THSD7B	Black
LETM2	Black
GFPT2	Black
KRT7	Black
LAPTM5	Black
FCER1G	Black
KLK7	Black
C1QB	Black
TRIP12	Black
UQCR10	Black
ELK4	Black
HIGD2A	Black
BATF	Black
MYO1F	Black
LYN	Black
LAIR1	Black
DEFA3	Black
DCSTAMP	Black
LRRC42	Black
C5orf46	Black
UBD	Black
SEMA7A	Black
ACTBL2	Black
PRAM1	Black
ARSH	Black
GSDMA	Black
IL4I1	Black
CCL26	Black
PIP5K1A	Black
CD80	Black
SHOX2	Black
NABP1	Black
OAS3	Black
ADAM17	Black
PRRG1	Black
ANXA3	Black
HK3	Black
LILRA2	Black
CAND1	Black
ITGAX	Black
MMD	Black
ASTE1	Black
ANO4	Black
FPR3	Black
SLAMF8	Black
ADAM19	Black
CYP1B1	Black
FCGR3A	Black
CCR8	Black
MORC4	Black
RASSF4	Black
ZNF768	Black
TYMP	Black
SLC2A3	Black
KCNH4	Black
KRT79	Black
COX6B1	Black
MYH6	Black
EMP2	Black
C2CD4A	Black
OSBPL8	Black
DNAH2	Black
SLC15A3	Black
LOC100506585	Black
CDC42SE1	Black
PICALM	Black
C9orf139	Black
TMEM86A	Black
TNFRSF9	Black
FASTK	Black
S100A9	Black
NFAM1	Black
TREM1	Black
LINC00256A	Black
ZMYND15	Black
C5AR1	Black
RXFP1	Black
FPR1	Black
CLEC12A	Black
LILRB2	Black
HNRPDL	Black
SLC1A3	Black
HNF1A-AS1	Black
CXCR1	Black
LILRB1	Black
MSR1	Black
FCAR	Black
ACP5	Black
TRAF1	Black

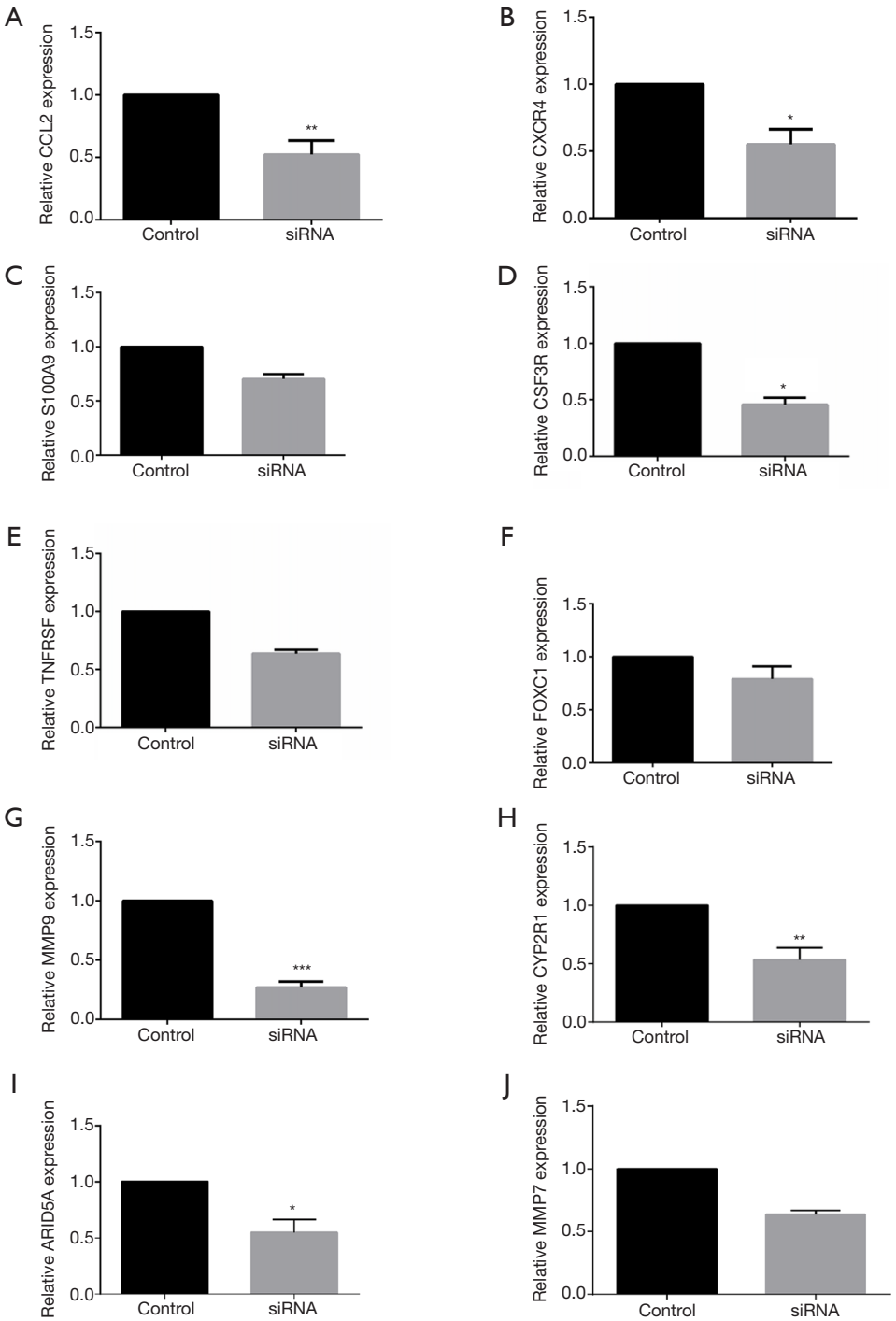

Figure S1 Ten hub genes expression (A: CCL2, B: CXCR4, C: S100A9, D: CSF3R, E: TNFRSF, F: FOXC1, G: MMP9, H: CYP2R1, I: ARID5A, J: MMP7) in si-FOXP3 group and control group. *, P<0.05; **, P<0.01; ***, P<0.001.